Geophysical research Letters

Supporting Information for

A reduction in marine primary productivity driven by rapid warming over the tropical Indian Ocean

Mathew Koll Roxy[1], Aditi Modi[1], Raghu Murtugudde[2], Vinu Valsala[1], Swapna Panickal[1], S. Prasanna Kumar[3], M. Ravichandran[4,5], Marcello Vichi[6,7] and Marina Lévy[8]

[1]Centre for Climate Change Research, Indian Institute of Tropical Meteorology, Pune, India, [2]ESSIC, University of Maryland, College Park, Maryland, USA, [3]CSIR-National Institute of Oceanography, Goa, India, [4]Indian National Centre for Ocean Information Services, Hyderabad, India, [5]National Centre for Antarctic and Ocean Research, Goa, India, [6]Department of Oceanography, University of Cape Town, Cape Town, South Africa, [7]Nansen-Tutu Centre for Marine Environmental Research, Cape Town, South Africa, [8]Sorbonne Université (UPMC, Paris 6/CNRS/IRD/MNHN), LOCEAN-IPSL,Paris, France

Contents of this file

Text S1 to S3
Figures S1 to S8
Table S1

Introduction

This supporting information provides further details on the observed data, CMIP5 historical simulations and the Earth System Model utilized in the study. It also includes additional figures validating the historical simulations with respect to observations, and the statistical techniques used. A detailed examination of the change in nutrients along with the changes in SST, stratification and chlorophyll is also provided.

Text S1.

Observed Data. Though marine primary production can be assessed directly using field flux measurements, chlorophyll pigment concentration measured through satellites is used as a convenient indicator of phytoplankton biomass and extent, as it represents the magnitude and variance in marine primary production and captures the first order changes in phytoplankton biomass [*Ryther and Yentsch*, 1957]. These satellite observations, which are mostly based on the visible bands of the radiance spectra (412-555 nm), lack consistent and accurate measurements of surface chlorophyll whenever cloudy conditions persist, which of course, is an integral part of the Asian summer monsoon season. Though seasonal and monthly mean composites can be derived from satellite data to some extent, it is challenging to derive robust signals of long-term trends of chlorophyll over the Indian Ocean because the current availability of satellite data is limited to a fairly short period since the satellite era [*Boyce et al.*, 2010; *Rykaczewski and Dunne*, 2011]. Studies suggest that the number of years required to detect a trend above the natural variability in most of the global oceans is 50-60 years, though a shorter period of 20-30 years could be used to extract the trends in the tropical oceans including the western Indian Ocean [*Beaulieu et al.*, 2013; *Henson et al.*, 2010]. The recently available satellite data blended from the multiple sensors of satellites bring the number of years of continuous data up to 16 years, bringing it close to the required trend detection time.

The chlorophyll data is obtained from version 2 of the European Space Agency's Ocean Color-Climate Change Initiative (OC-CCI) [*Sathyendranath et al.,* 2016]. The OC-CCI uses processors for atmospheric correction and retrieval of in-water properties on the basis of round-robin comparison of candidate algorithms [*Brewin et al.,* 2015; *Müller et al.,* 2015]. The OC-CCI chlorophyll product is generated from merged normalized remote-sensing reflectances from SeaWiFS, MODIS-Aqua, and MERIS satellites at 4 km-by-4 km horizontal resolution, band shifted to SeaWiFS wavebands. The POLYMER algorithm used by OC-CCI for processing MERIS data [*Steinmetz et al.,* 2011] is able to retrieve usable data under sun-glint conditions, which improves the coverage in the Arabian Sea, especially during the summer monsoons. The OC-CCI data is available for the period 1998-2013. However, the last couple of years (2012 and 2013) suffer from data gaps (less than 50% coverage) in the Arabian Sea, which could introduce spurious trends. These two years are presented in the analysis for an overview, but are not utilized for estimating the trends and correlation coefficients in the current analysis.

In order to validate the robustness of the satellite data, *in-situ* data from Teledyne/Webb APEX - Argo floats deployed in the Arabian Sea are used [*Ravichandran et al.*, 2012]. These floats were equipped with WETLabs ECO FLNTU package for measuring chlorophyll-a fluorescence (470 nm) with an accuracy of 0.02 mg m^{-3}. The chlorophyll was measured from about 10 m to 2000 m depth, with a vertical resolution of about 5 m in the top 150 m. OC-CCI data is averaged over a region within the trajectories of the Argo floats (60-70°E, 5-15°N) and compared for the period during which *in-situ* data is available (year 2010). It should be taken into account that while the OC-CCI data represents satellite measurements at the sea surface, the *in-situ* data used for comparison is at about 10 m depth. Also, the *in-situ* data is measured at daily intervals, capturing fine details of the variability. Regardless of these limitations, both the time series show a high correlation (r = 0.92), statistically significant at 95% confidence level (Figure S1). There are slight discrepancies in the magnitude, which are probably due to the differences in the depth, frequency and location of these measurements. Nevertheless, OC-CCI captures the seasonal variability of the chlorophyll anomalies in the Indian Ocean with high fidelity, and indicates that it is useful for examining the climate driven trends in the basin.

Hydrographic data including SST and density are obtained from the Hadley Centre EN4 dataset containing Argo observations. Ocean stratification is estimated from the density difference between the surface and a depth of 200m, using a stability parameter,

$$E = -\frac{1}{\rho}\frac{\partial \rho}{\partial z},$$

where E is the static stability parameter (m^{-1}), ρ is the density (kg m^{-3}) of the water and z is the depth (m) [*Behrenfeld et al.*, 2006; *Narvekar and Prasanna Kumar*, 2014].

Sea surface (10 m) wind speed at 0.25° grid resolution is obtained from the multi-satellite blended sea winds provided by NOAA/NCDC. Wind stress curl is estimated using

$$\nabla X\tau = \frac{\partial \tau_y}{\partial x} - \frac{\partial \tau_x}{\partial y}$$

where $\tau_x$and τ_{xy} denote the eastward and northward components of wind stress. A positive wind stress curl indicates wind induced upwelling, and vice-versa.

Text S2.

CMIP5 Historical Simulations. In order to ascertain the role of a warming Indian Ocean on the long-term chlorophyll trends, a suite of historical simulations by earth system models participating in the Coupled Model Intercomparison Project (CMIP5) are used (Table S1). These historical simulations are compared with the observations for the same period (1998-2005) for their ability to reproduce the spatial distribution of mean climatology and interannual variability of chlorophyll concentrations in the Indian Ocean (Figures S2-S4). Five good models are selected based on their skills in realistic simulation of the mean and variability and pattern correlations (r > 0.4) over the north Indian Ocean. Ensemble means of these five models, namely the NOAA-GFDL-ESM2M, NOAA-GFDL-ESM2G, MPI-ESM-LR, MPI-ESM-MR and IPSL-CM5A-MR are used to examine the trends in the chlorophyll concentrations. Pattern correlation coefficients (PCC) computed between the summer mean chlorophyll values simulated by the models and the observations for the same period for the north Indian Ocean (50-100°E, 5-25°N) exhibits the highest correlation coefficients for the MPI-ESMs (r > 0.5), larger than the PCC for the ensemble mean (r = 0.39). This means that the MPI-ESMs behave like the ensemble, but have a larger fidelity in representing the spatial distribution of chlorophyll variability in the Indian Ocean.

MPI-ESMs simulate the mean climatology of chlorophyll concentrations with less bias and realistic spatial distribution in the Indian Ocean, particularly in the Arabian Sea where the primary production as well as the surface warming is most prominent. However, the model has an obvious positive bias in the simulated chlorophyll concentrations in the equatorial Indian Ocean. This could be due to a model misinterpretation of the equatorial dynamics in this region—as upwelling driven by equatorial easterlies are not a robust feature of the Indian Ocean—which climate models very often fail to reproduce [*McCreary et al.*, 2009]. Among the two versions of MPI-ESMs used here, the lower-resolution (LR, r = 0.59) exhibits a pattern correlation higher than that of the higher-resolution (MR, r = 0.50). However, the higher-resolution model is chosen for further analysis as it has relatively lesser bias in most of the Indian Ocean including the equatorial regions, as well as the Bay of Bengal and western Indian Ocean (Figure S3). Also, MPI-ESM-MR features one of the highest ocean resolutions (0.4˚) among all the available CMIP5 models, and the temperature biases are smaller in MR, compared to LR. The MR version of MPI-ESM doubles the number of levels in the atmosphere from 47 to 95 and decreases the horizontal grid spacing of the ocean from nominally 1.5° to 0.4°, hence, featuring a quasi-uniform, eddy-permitting global resolution, compared to the LR configuration [*Jungclaus et al.*, 2013]. Hence MPI-ESM-MR is used as a representative model, based on the selected set of CMIP5 historical simulations, for extensive process study.

The MPI-ESM-MR model is found to be skillful in simulating the mean state of the physical variables including SST and winds in the Indian Ocean [*Prasanna*, 2015], which are crucial in driving the chlorophyll variability on both interannual and long-term climate time scales in a basin which is monsoon driven (Figure S5). Pattern correlations between the model simulations and observations yield significant correlation coefficients for SST (r = 0.88), winds (r = 0.95) and static stability (r = 0.93), at 95% confidence levels. The model skillfully simulates the magnitude (maximum 1.0°C and above) and spatial distribution of the observed Indian Ocean SST trends during 1950-2005, with the maximum warming spread over the west-central Indian Ocean (Arabian Sea) and minimum over the southeastern part of the basin. Historical data of chlorophyll, SST, winds and density for the period 1950-2005, simulated by MPI-ESM-MR is utilized to examine the climate driven trends in marine primary productivity.

It is however to be cautioned that CMIP5 historical simulations have some obvious limitations. Firstly, they are not hindcasts, but simulations forced with the historical changes in greenhouse gas mixing ratios (radiative forcing). CMIP5 models are typically spun up for the pre-industrial CO_2 levels and integrated forward and thus possess their own internal variability when it comes to seasonal-to-interannual and longer timescale variabilities with no correspondence to actual events such as El Niño-Southern Oscillation (ENSO) or Indian Ocean Dipole (IOD) in observations. Hence the historical simulations of chlorophyll would represent the response to increasing temperatures alone, but will not have the year-to-year variability as in observations (to be precise, coincident interannual variability). These CMIP5 simulations can hence be compared for climatologies and trends but not for year-to-year variabilities. Secondly, while the observations are of very high spatial resolution (less than 0.1° at source, 0.25° used here) and include small scale variabilities, the model historical simulations are of relatively lower resolution (0.4°~0.5°) and have a low skill in resolving sub-mesoscale eddies which are prominent in these regions. This means that while the model will be able to represent trends and variabilities on a large spatial scale, it will not be able to do so for small regions.

Marine biogeochemistry in MPI-ESM is represented by the Hamburg Ocean Carbon Cycle (HAMOCC) model [*Ilyina et al.*, 2013]. HAMOCC simulates the oceanic carbon cycles along with other biogeochemical elements, and prognostically computes up to seventeen tracers in the water column. Marine biology dynamics in HAMOCC is based on an extended NPZD (nutrient, phytoplankton, zooplankton and detritus) model, which connects biogeochemical cycles and trophic levels through the uptake of nutrients and re-mineralization of organic matter. Phytoplankton growth in the model follows Michaelis-Menten kinetics, and depends on temperature, light, and nutrient availability. Inorganic carbon chemistry in HAMOCC mainly follows Maier-Reimer and Hasselmann [1987] with a revised estimation of chemical constants [*Goyet and Poisson*, 1989]. HAMOCC also incorporates a simplified marine sulfur cycle which includes the production, bacterial consumption, photolysis, and sea-air gas exchange of dimethylsulphide.

Text S3.

IITM Earth System Model. In order to delineate the causal role of SST warming on the nutrient mixing and the chlorophyll concentrations, a sensitivity experiment using the standard configuration of an earth system model with interactive biogeochemistry, the IITM-ESM [*Swapna et al.*, 2015] is used. The oceanic component (GFDL MOM4p1) has a 0.25–0.5° horizontal resolution, 40 vertical levels and includes an ice model. The atmospheric component (NCEP GFS) is at T126 (~0.9°) horizontal resolution and 64 sigma-pressure hybrid levels. The oceanic component is coupled with a biogeochemistry module, TOPAZ [*Dunne et al.*, 2010]. The model exhibits reasonable skills in simulating the monsoonal characteristics over the Indian Ocean, including that of SST and chlorophyll [*Swapna et al.*, 2015]. The coupled configuration of IITM-ESM is time integrated over a period of 50 years, and serves as the reference run (ESM_{CTL}). Ensembles (10 members) of short integrations for 10 different summer monsoon seasons (June-September) from the (ESM_{CTL}) were performed by adding temperature anomalies to the SSTs in the Indian Ocean (ESM_{IO}). Positive anomalies of the order of 1.5°C was added over the region, in such a way that it tapers out by the limits of the domain (50-65°E, 5°S-10°N). The difference between ESM_{IO} and ESM_{CTL} is taken as the model chlorophyll response to the summer warming over the Indian Ocean. Figure S6 shows the model-simulated chlorophyll anomalies in response to a warming simulated over the western Indian Ocean. The response corresponds to an SST increase of about 1.0°C added to the entire Indian Ocean basin to represent the basin-wide warming, with a maximum increase of 1.5°C in the west-central region, similar to the observed trends during the northern summer.

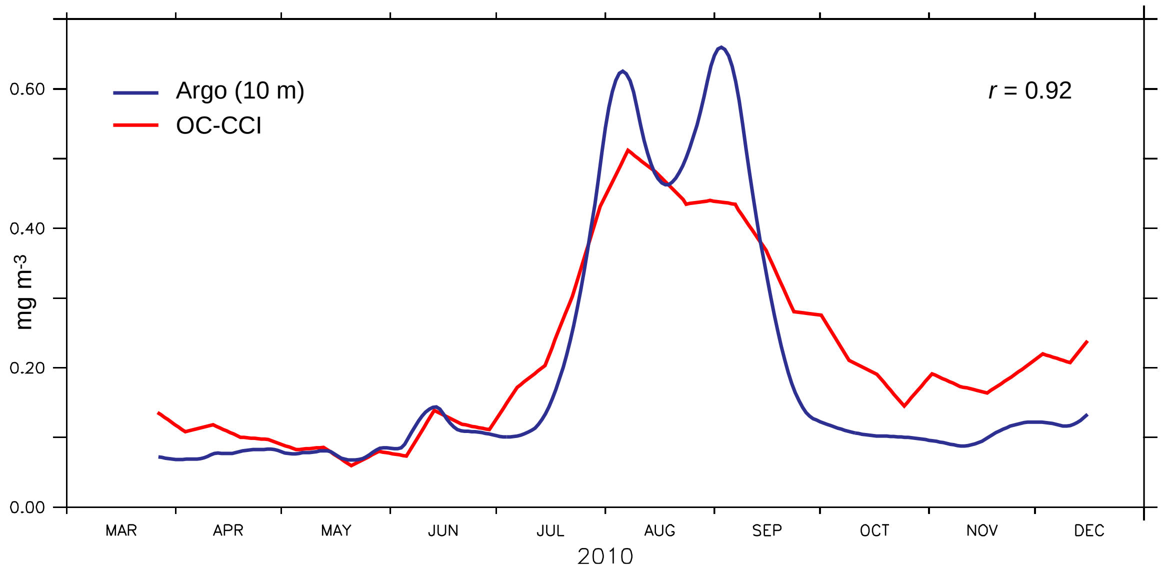

Figure S1. Temporal evolution of chlorophyll-a (mg m^{-3}) during the year 2010, derived from an Argo float at 10 m depth (blue) and OC-CCCI data (red) for a region where the data points coincide in the Arabian Sea (60-70°E, 5-15°N). The correlation coefficient (r = 0.92) is significant at 95% confidence level, using a standard two-tailed Student's t-test.

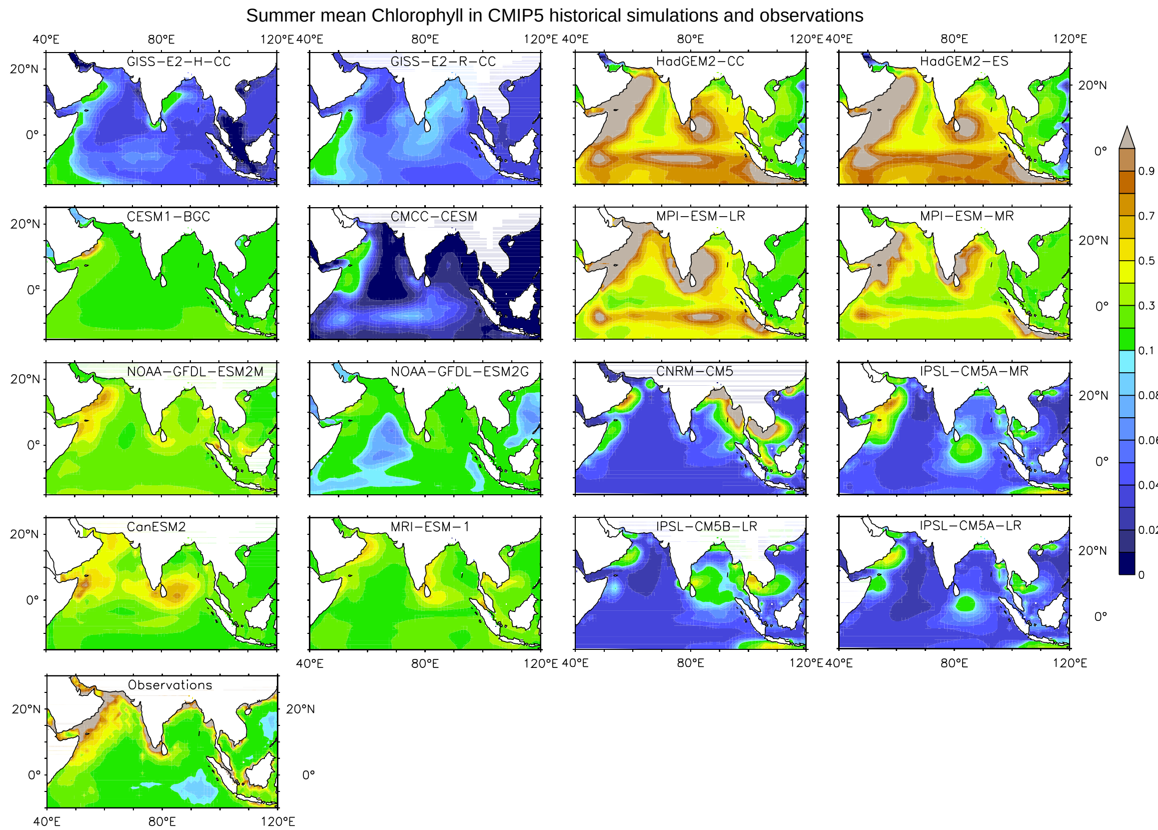

Figure S2. Climatology of June-September mean chlorophyll concentration distribution obtained from CMIP5 models and observations, for the years 1998-2005.

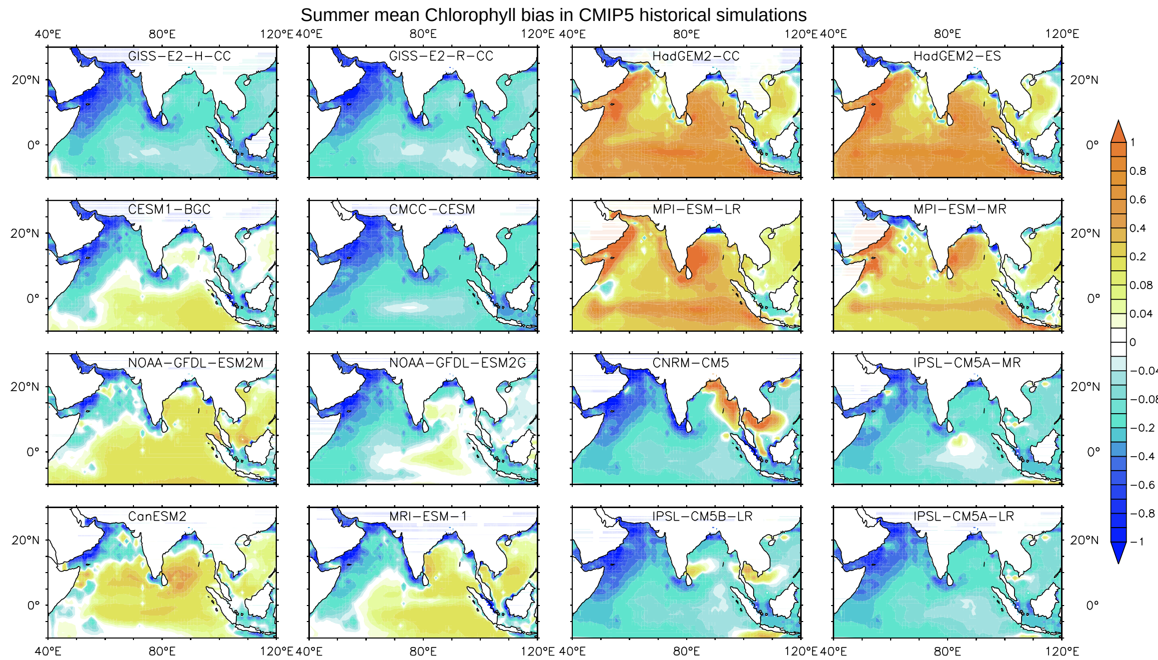

Figure S3. Bias (model – observations) in the CMIP5 simulations mean chlorophyll concentration distribution, for the years 1998-2005.

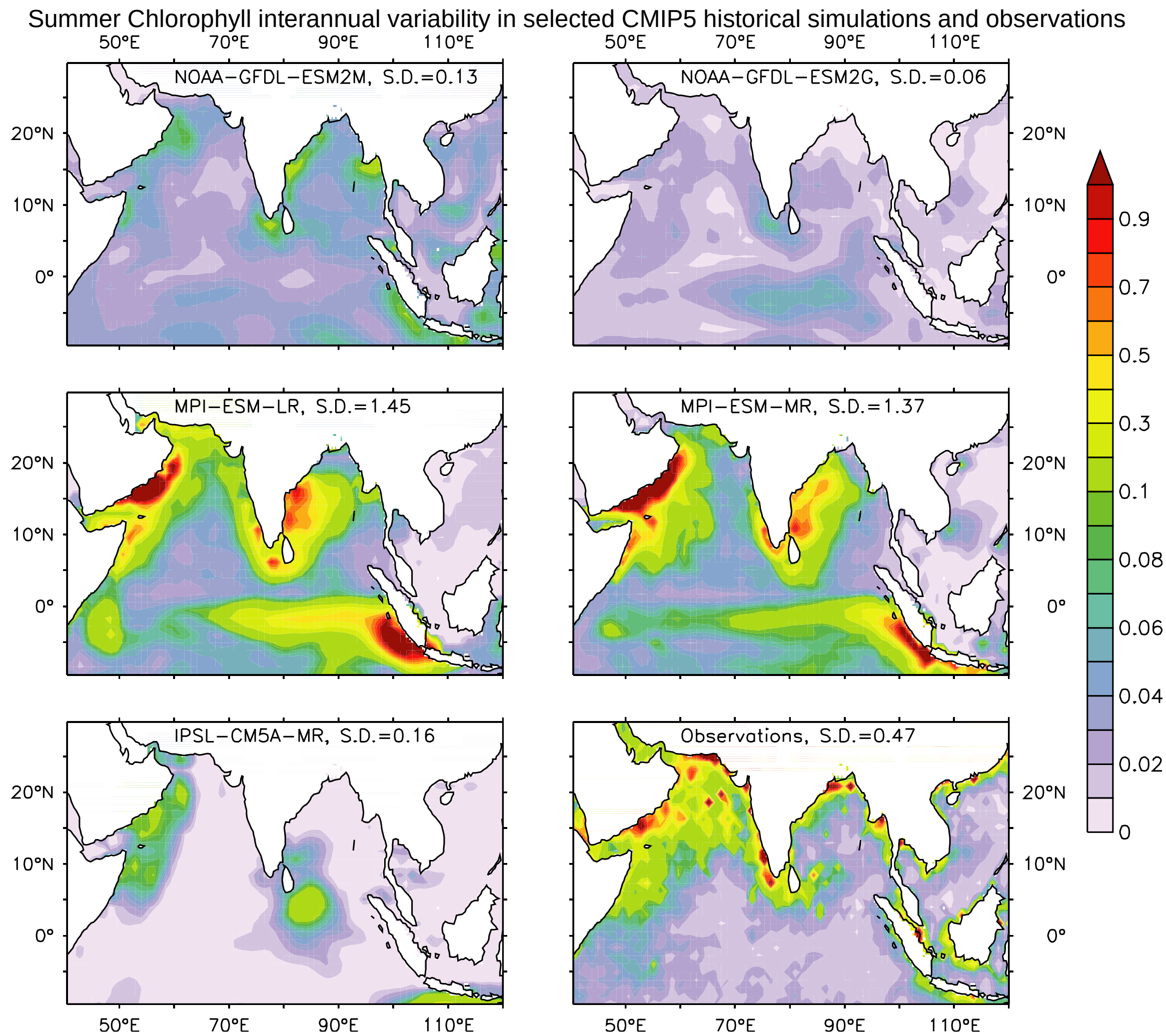

Figure S4. Interannual variability in June-September mean chlorophyll concentration distribution obtained from the selected CMIP5 historical simulations and observations, for the years 1998-2005.

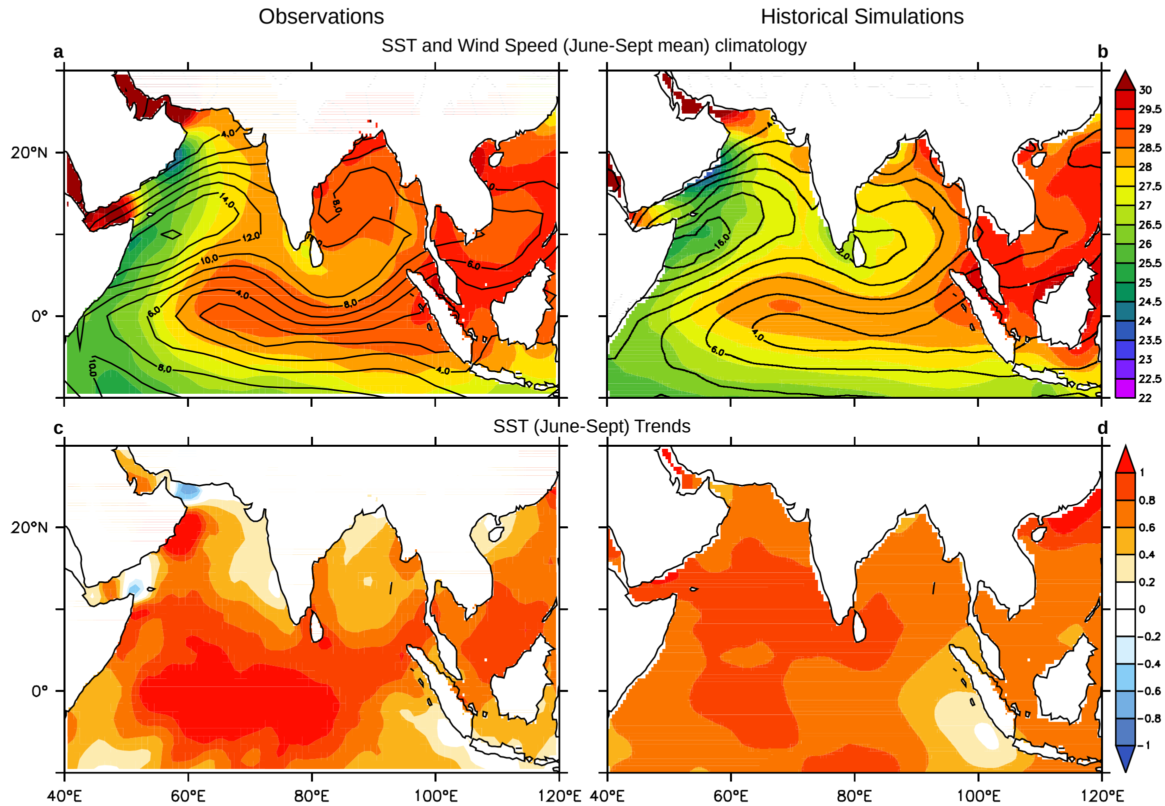

Figure S5. Climatology of June-September (a, b) mean SST (colors, °C) and wind speed (contours, m s^{-1}), and (c, d) SST trends (°C per 56 years), obtained from observations and MPI-ESM-MR historical simulations, for the years 1950-2005. Color shades in c and d denote trends that are significant at 95% confidence levels.

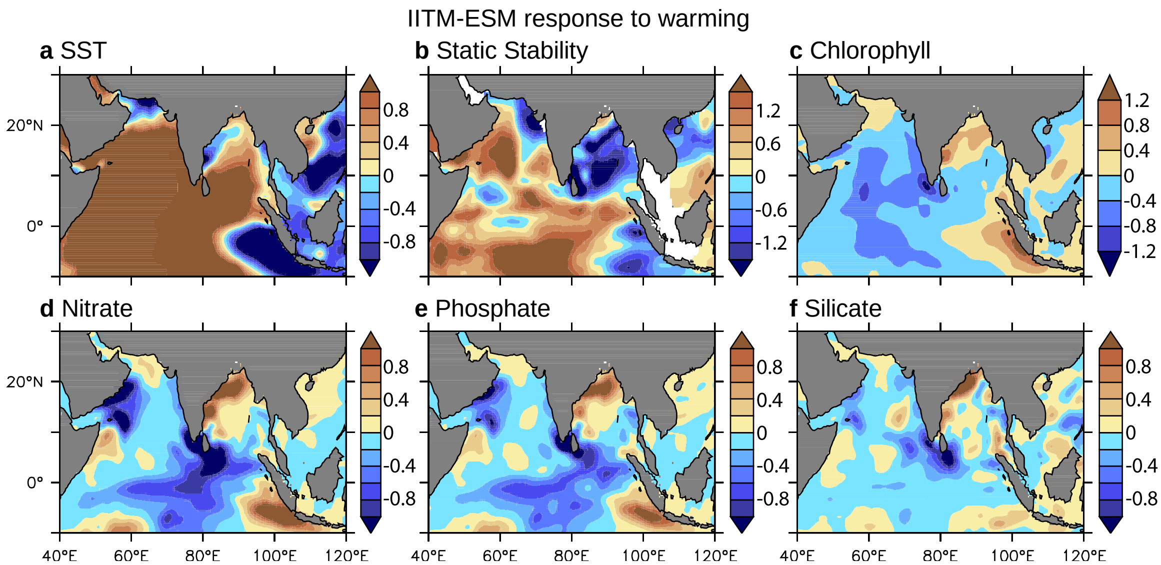

Figure S6. Model simulated (a) SST (°C), (b) static stability, (c) chlorophyll (mg m^{-3}), and (d-f) nitrate (µmol L^{-1}), phosphate (10^{-1} µmol L^{-1}) and silicate (µmol L^{-1}) anomalies in response to warming over the Indian Ocean, for June-September. The model simulated anomalies are estimated from the sensitivity run where SST anomalies of the order of 1.5°C is introduced over the western Indian Ocean (CFSv2$_{IO}$), with respect to a model control run (CFSv2$_{CTL}$).

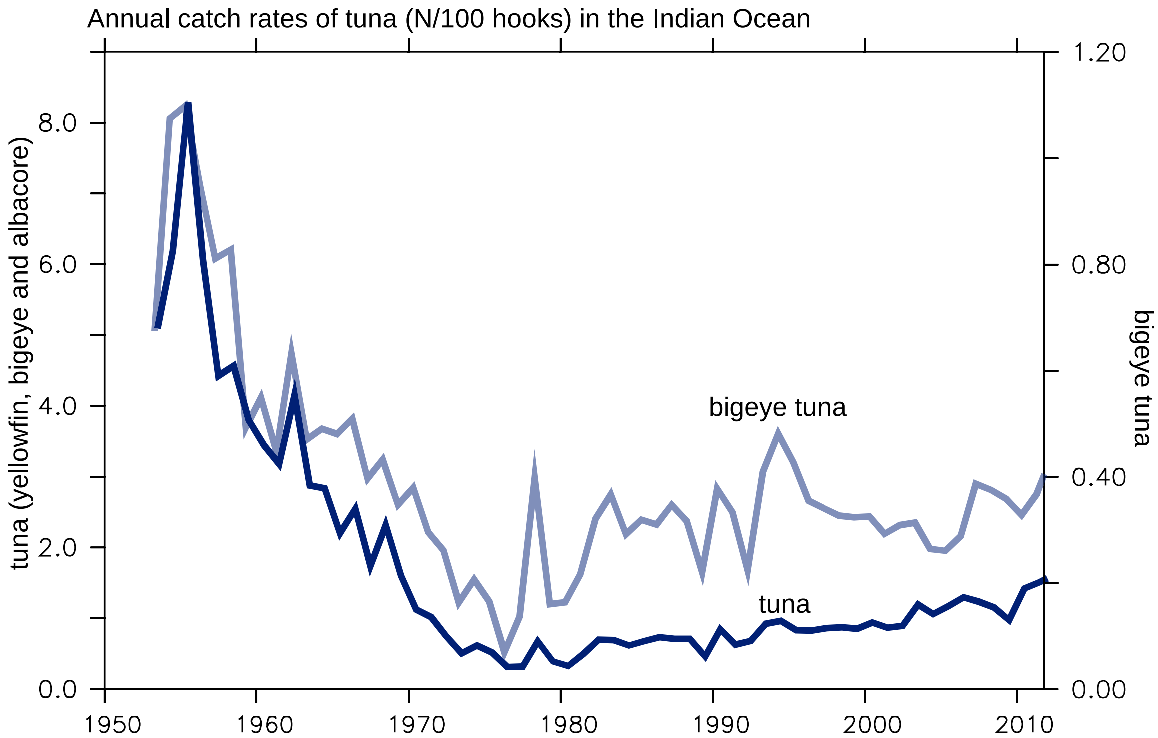

Figure S7. Annual catch rates (N/100 hooks) for the three principle species of tuna which comprises of 75% of all fishery products, caught by Japanese long-liners in the Indian Ocean. Data is obtained from the Indian Ocean Tuna Commission (IOTC).

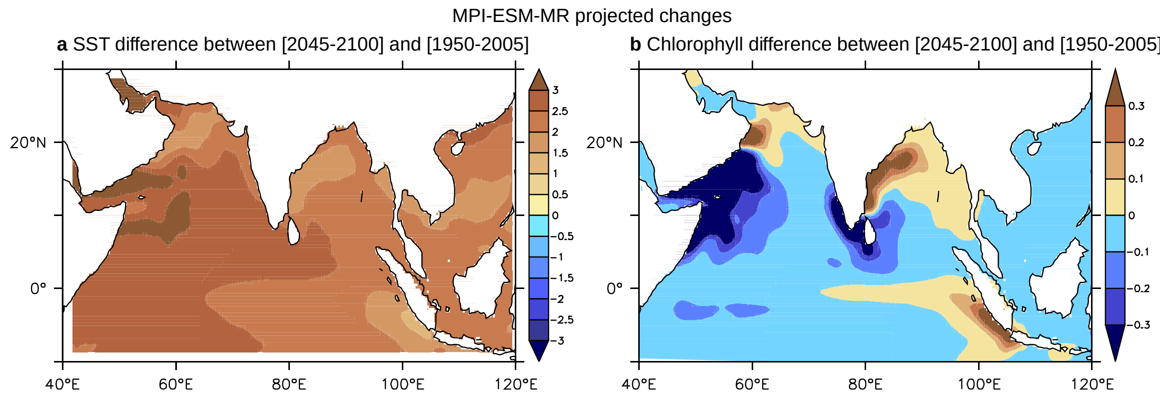

Figure S8. Difference in summer (a) SST (°C) and (b) chlorophyll (mg m^{-3}), between future projections (2045-2100) and historical simulations (1950-2005) of MPI-ESM-MR.

#	CMIP5 Model	Atmosphere	Ocean	Ocean BGC	Reference	PCC
1	GISS-E2-H-CC	40 lev, 2.5°/2°	26 lev, 1°/1°	NOBM	*Gregg and Casey*	0.21
2	GISS-E2-R-CC	40 lev, 2.5°/2°	32 lev, 1.25°/1°	NOBM	*Gregg and Casey*	0.09
3	CESM1-BGC	26 lev, 0.25°/0.94°	60 lev, 1.125°/0.27° -0.53°	BEC	*Moore et al.* [2004]	0.27
4	CMCC-CESM	39 lev, 3.8°	31 lev, 0.5-2°	PELAGOS	*Vichi et al.* [2007]	0.39
5	NOAA-GFDL-ESM2M	24 lev, 2.5°/2.0°	50 lev, 0.3-1°	TOPAZ2	*Dunne et al.* [2013]	0.44
6	NOAA-GFDL-ESM2G	24 lev, 2.5°/2.0°	63 lev, 0.3-1°	TOPAZ2	*Dunne et al.* [2013]	0.44
7	CanESM2	35 lev, 2.8°/2.8°	40 lev, 1.4°/0.9°	NPZD [*Denman and Pena*, 1999]	*Zahariev et al.* [2008]	0.33
8	MRI-ESM1	23 lev.1.125°/1.12	51 lev, 1°/0.5°	NPZD [*Oschlies*, 2001]	*Adachi et al.* [2013]	0.06
9	HadGEM2-CC	60 lev, 1.2°/1.9°	40 lev, 1°/0.3-1°	Diat-HadOCC	*Palmer and Totterdell* [2001]	0.37
10	HadGEM2-ES	38 lev, 1.2°/1.9°	40 lev, 1°/0.3-1°	Diat-HadOCC	*Palmer and Totterdell* [2001]	0.37
11	MPI-ESM-LR	47 lev, 1.9°	40 lev, 1.5°	HAMOCC5.2	*Ilyina et al.* [2013]	0.59
12	MPI-ESM-MR	95 lev, 1.9°	40 lev, 0.4°	HAMOCC5.2	*Ilyina et al.* [2013]	0.50
13	CNRM-CM5	31 lev, 1.4°	42 lev, 1°	PISCES	*Séférian et al.* [2013]	0.03
14	IPSL-CM5A-MR	39 lev, 1.2°/2.5°	31 lev, 2°/0.5-2°	PISCES	*Séférian et al.* [2013]	0.48
15	IPSL-CM5B-LR	39 lev, 1.2°/2.5°	31 lev, 2°/0.5-2°	PISCES	*Séférian et al.* [2013]	0.15
16	IPSL-CM5A-LR	39 lev, 1.9°/3.8°	31 lev, 2°/0.5-2°	PISCES	*Séférian et al.* [2013]	0.39

Table S1. Details of the CMIP5 models having ocean biogeochemistry (BGC) component, providing historical simulations of chlorophyll concentration. Pattern correlation coefficient (PCC) between climatological summer means of the observations and CMIP5 historical simulations for chlorophyll concentrations during the period 1998-2005 is provided in the last column.

References.

Adachi, Y., S. Yukimoto, M. Deushi, A. Obata, H. Nakano, T. Y. Tanaka, M. Hosaka, T. Sakami, H. Yoshimura, and M. Hirabara (2013), Basic performance of a new earth system model of the Meteorological Research Institute (MRI-ESM1), *Papers in Meteorology and Geophysics*, *64*, 1-19.

Beaulieu, C., S. A. Henson, J. L. Sarmiento, J. P. Dunne, S. C. Doney, R. Rykaczewski, and L. Bopp (2013), Factors challenging our ability to detect long-term trends in ocean chlorophyll, *Biogeosciences*, *10*, 2711–2724.

Behrenfeld, M. J., R. T. O'Malley, D. A. Siegel, C. R. McClain, J. L. Sarmiento, G. C. Feldman, A. J. Milligan, P. G. Falkowski, R. M. Letelier, and E. S. Boss (2006), Climate-driven trends in contemporary ocean productivity, *Nature*, *444*(7120), 752-755.

Boyce, D. G., M. R. Lewis, and B. Worm (2010), Global phytoplankton decline over the past century, *Nature*, *466*(7306), 591-596.

Brewin, R. J., D. E. Raitsos, G. Dall'Olmo, N. Zarokanellos, T. Jackson, M.-F. Racault, E. S. Boss, S. Sathyendranath, B. H. Jones, and I. Hoteit (2015), Regional ocean-colour chlorophyll algorithms for the Red Sea, *Remote Sensing of Environment*, *165*, 64-85.

Denman, K., and M. Pena (1999), A coupled 1-D biological/physical model of the northeast subarctic Pacific Ocean with iron limitation, *Deep Sea Research Part II: Topical Studies in Oceanography*, *46*(11), 2877-2908.

Dunne, J. P., A. Gnanadesikan, J. L. Sarmiento, and R. D. Slater (2010), Technical description of the prototype version (v0) of tracers of phytoplankton with allometric zooplankton (TOPAZ) ocean biogeochemical model as used in the Princeton IFMIP model, *Biogeosciences*, *7*, 3593.

Dunne, J. P., J. G. John, E. Shevliakova, R. J. Stouffer, J. P. Krasting, S. L. Malyshev, P. Milly, L. T. Sentman, A. J. Adcroft, and W. Cooke (2013), GFDL's ESM2 Global Coupled Climate–Carbon Earth System Models. Part II: Carbon System Formulation and Baseline Simulation Characteristics*, *Journal of Climate*, *26*(7), 2247-2267.

Goyet, C., and A. Poisson (1989), New determination of carbonic acid dissociation constants in seawater as a function of temperature and salinity, *Deep Sea Research Part A. Oceanographic Research Papers*, *36*(11), 1635-1654.

Gregg, W. W., and N. W. Casey (2007), Modeling coccolithophores in the global oceans, *Deep Sea Research Part II: Topical Studies in Oceanography*, *54*(5), 447-477.

Henson, S. A., J. L. Sarmiento, J. P. Dunne, L. Bopp, I. D. Lima, S. C. Doney, J. John, and C. Beaulieu (2010), Detection of anthropogenic climate change in satellite records of ocean chlorophyll and productivity, *Biogeosciences*, *7*, 621-640.

Ilyina, T., K. D. Six, J. Segschneider, E. Maier-Reimer, H. Li, and I. Núñez-Riboni (2013), Global ocean biogeochemistry model HAMOCC: Model architecture and performance as component of the MPI-Earth system model in different CMIP5 experimental realizations, *Journal of Advances in Modeling Earth Systems*, *5*(2), 287-315.

Jungclaus, J., N. Fischer, H. Haak, K. Lohmann, J. Marotzke, D. Matei, U. Mikolajewicz, D. Notz, and J. Storch (2013), Characteristics of the ocean simulations in the Max Planck Institute Ocean Model (MPIOM) the ocean component of the MPI-Earth system model, *Journal of Advances in Modeling Earth Systems*, *5*(2), 422-446.

Maier-Reimer, E., and K. Hasselmann (1987), Transport and storage of CO2 in the ocean——an inorganic ocean-circulation carbon cycle model, *Climate dynamics*, *2*(2), 63-90.

McCreary, J., R. Murtugudde, J. Vialard, P. Vinayachandran, J. D. Wiggert, R. R. Hood, D. Shankar, and S. Shetye (2009), Biophysical processes in the Indian Ocean, *Indian Ocean Biogeochemical Processes and Ecological Variability*, 9-32.

Moore, J. K., S. C. Doney, and K. Lindsay (2004), Upper ocean ecosystem dynamics and iron cycling in a global three-dimensional model, *Global Biogeochemical Cycles*, *18*(4).

Müller, D., H. Krasemann, R. J. Brewin, C. Brockmann, P.-Y. Deschamps, R. Doerffer, N. Fomferra, B. A. Franz, M. G. Grant, and S. B. Groom (2015), The Ocean Colour Climate Change Initiative: I. A methodology for assessing atmospheric correction processors based on in-situ measurements, *Remote Sensing of Environment*, *162*, 242-256.

Narvekar, J., and S. Prasanna Kumar (2014), Mixed layer variability and chlorophyll a biomass in the Bay of Bengal, *Biogeosciences*, *11*, 3819-3843.

Oschlies, A. (2001), Model-derived estimates of new production: New results point towards lower values, *Deep Sea Research Part II: Topical Studies in Oceanography*, *48*(10), 2173-2197.

Palmer, J., and I. Totterdell (2001), Production and export in a global ocean ecosystem model, *Deep Sea Research Part I: Oceanographic Research Papers*, *48*(5), 1169-1198.

Prasanna, V. (2015), Assessment of South Asian Summer Monsoon Simulation in CMIP5-Coupled Climate Models During the Historical Period (1850–2005), *Pure and Applied Geophysics*, 1-24.

Ravichandran, M., M. Girishkumar, and S. Riser (2012), Observed variability of chlorophyll-a using Argo profiling floats in the southeastern Arabian Sea, *Deep Sea Research Part I: Oceanographic Research Papers*, *65*, 15-25.

Rykaczewski, R. R., and J. P. Dunne (2011), A measured look at ocean chlorophyll trends, *Nature*, *472*(7342), E5-E6.

Ryther, J. H., and C. Yentsch (1957), The estimation of phytoplankton production in the ocean from chlorophyll and light data, *Limnology and oceanography*, 281-286.

Sathyendranath, S., et. al. (2016), Creating an ocean-colour time series for use in climate studies: the experience of the ocean-colour climate change initiative, *Remote Sensing of Environment*, Submitted.

Séférian, R., L. Bopp, M. Gehlen, J. C. Orr, C. Ethé, P. Cadule, O. Aumont, D. S. y Mélia, A. Voldoire, and G. Madec (2013), Skill assessment of three earth system models with common marine biogeochemistry, *Climate Dynamics*, *40*(9-10), 2549-2573.

Steinmetz, F., P.-Y. Deschamps, and D. Ramon (2011), Atmospheric correction in presence of sun glint: application to MERIS, *Optics express*, *19*(10), 9783-9800.

Swapna, P., M. Roxy, K. Aparna, K. Kulkarni, A. Prajeesh, K. Ashok, R. Krishnan, S. Moorthi, A. Kumar, and B. Goswami (2015), The IITM Earth System Model: Transformation of a Seasonal Prediction Model to a Long Term Climate Model, *Bulletin of the American Meteorological Society*.

Vichi, M., N. Pinardi, and S. Masina (2007), A generalized model of pelagic biogeochemistry for the global ocean ecosystem. Part I: Theory, *Journal of Marine Systems*, *64*(1), 89-109.

Zahariev, K., J. R. Christian, and K. L. Denman (2008), Preindustrial, historical, and fertilization simulations using a global ocean carbon model with new parameterizations of iron limitation, calcification, and N 2 fixation, *Progress in Oceanography*, *77*(1), 56-82.